The International Journal of Advanced Manufacturing Technology (2023) 127:3665–3680
https://doi.org/10.1007/s00170-023-11773-8

ORIGINAL ARTICLE

Process chain for the mass production of polymeric microfluidic chips

Yanjun Lu[1] · Bo Liu[1] · Zili Zhang[2] · Mingrong Guo[1] · Jianjian Wang[3,4] · Chunjin Wang[2]

Received: 16 February 2023 / Accepted: 9 June 2023 / Published online: 17 June 2023

Abstract
The moulding process is a low-cost method for the mass production of microfluidic chips, rather than fabricating the chips one by one. The precision manufacturing of the mould is the key to the moulding process, which usually includes a combination of several machining processes. However, most of the current studies focus on a single process in microfluidic chip fabrication, which makes it difficult to optimise the fabrication process, resulting in low production efficiency and high energy consumption. Therefore, to realize the low cost and sustainable mass production of microfluidic chips, the process chain is developed in this paper. The process chain includes milling, precision ultrasonic vibration–assisted grinding, fluid jet polishing, and injection moulding. Parametric experiments regarding the key parameters of grinding, polishing, and injection moulding are conducted to obtain the optimization conditions. The form accuracy of the microchannel reaches 8.594 μm, and the roughness at the bottom surface of the microchannel is 0.027 μm. The experimental results demonstrate that the proposed process chain is effective and feasible for the mass production of microfluidic chips with high surface quality. It also provides some theoretical bases for the manufacturing of structured surfaces with nanometric surface roughness.

Keywords Microfluidic chip · Process chain · Grinding · Milling · Fluid jet polishing · Ultra-precision machining

1 Introduction

Microfluidic technology has developed rapidly in recent years, from the initial field of analytical chemistry to bioanalysis, diagnostics [1], drug discovery [2], food processing [3], and many other fields. However, high surface quality and form accuracy are needed for the application of microfluidic chips with high performance. The high requirement poses a great challenge to the manufacturing of microfluidic chips, especially considering the small structures. Wang et al. [4] fabricated microchannel structures with a width of 200 μm in quartz by picosecond laser. He et al. [5] introduced the micro- and nano-processing of glass 3D structures using femtosecond laser direct writing processing technology. The microchannel with a width of about 40 nm and a length of 40 μm was fabricated, which can be used for micro-/nanofluid biosensors, photo fluidic sensors, current element sensors, and surface-enhanced Raman scattering equipment with high added value. However, the high manufacturing cost of laser processing restricts its processed products from being widely used in microfluidic chips. The efficiency of the microfluidic manufacturing process based on the chemical etching process is limited by the reaction rate at a low level, which has been improved after several years of development. Peng et al. [6] reported a simple and low-cost method for fabricating microchannels on silicon substrates using direct ink writing as a stable mask and metal-assisted chemical etching. However, the chemical liquids used in the process, specially buffered hydrofluoric acid, were harmful to the environment and require further treatment before emission [7]. Ku et al. [8] proposed a processing method for glass microfluidic devices by immersing the glass substrate in cold water by micro-milling, realising the manufacturing of microchannels with a depth of 50 μm and a width of 300 μm. This method can effectively remove debris and

✉ Chunjin Wang
chunjin.wang@polyu.edu.hk

1 Guangdong Key Laboratory of Electromagnetic Control and Intelligent Robots, College of Mechatronics and Control Engineering, Shenzhen University, Shenzhen 518060, China

2 State Key Laboratory of Ultra-Precision Machining Technology, Department of Industrial and Systems Engineering, The Hong Kong Polytechnic University, Hung Hom, Kowloon, Hong Kong, China

3 State Key Laboratory of Tribology in Advanced Equipment, Tsinghua University, Beijing 100084, China

4 Department of Mechanical Engineering, Tsinghua University, Beijing 10084, China

extend the service life of milling tools, but the chip is still fabricated one by one which is difficult for mass production.

To improve the production efficiency, different methods have been proposed in recent decades. Polymers, such as polypropylene (PP), methyl methacrylate (PMMA), and polydimethylsiloxane (PDMS), are inexpensive and easily manufactured in volume. Hence, polymers have become the most commonly used materials for microfluidic chips [9]. The forming technology of polymer materials is an effective means of microfluidic product mass production. At present, the main forming technologies are 3D printing technology [10], hot pressing technology [11], and microinjection moulding technology [12]. Tiboni et al. [13] manufactured two kinds of microfluidic chips using polypropylene and applied them to the manufacturing of nanomedicine. 3D printing technology can greatly shorten the manufacturing process of microfluidic chips and meet the demand for small quantities of microfluidic chips with various complex structures. However, 3D printing technology is currently facing a success rate problem, resulting in high material waste and energy waste [14]. As a result, hot embossing and injection moulding are the most widely used methods in the industry [15]. Lin et al. [16] replicated microfluidic channels in PMMA by hot embossing and found that microchannels had good characteristic integrity and replication quality through a fluidity test. However, hot pressing requires a heating stage every time, and the forming cycle is long. The advantages of the microinjection moulding technology lie in the lower requirements for mould strength, longer mould life, higher production efficiency of microfluidic chips, and relatively low cost. Hence, microinjection moulding technology has a great potential to be applied in the mass production of microfluidic chips with low cost.

The performance of microfluidic chips obtained by microinjection moulding technology depends on the surface quality and form accuracy of the microstructure mould core. The micro-nano structure manufacturing in the microfluidic chip mould core mainly relies on laser beam processing [17], chemical etching [18], lithography technology [19], electrical discharge machining (EDM) [20, 21], and micro-milling [22]. Wang et al. [23] used picosecond laser processing technology to fabricate micro-convex block arrays with a diameter of 12.5 μm, height of about 21.9 μm, and spacing of 25 μm. Wang et al. [24] created a two-scale layered surface structure with a two-dimensional regular array of microbumps with nano-ripples on the nickel surface. However, as a guarantee of the machining accuracy of microstructure, ultra-fast laser power directly affects the machining efficiency, and there are still many problems such as high energy consumption and high technical difficulty. Gan et al. [25] proposed the use of femtosecond laser-induced chemical etching to produce micro-moulds based on triangular diffraction gratings. Guo et al. [26] proposed a method for manufacturing 100-nm concave two-dimensional silicon nano-moulds by side etching stripping, which can produce high-precision and large-size silicon nano-moulds. However, it is still very difficult to chemically etch microstructure with a high aspect ratio. Iwai et al. [27] fabricated microfluidic devices using multi-layer soft lithography and injection moulding processes and verified droplet formation performance. Ayoib et al. [28] used an inkjet transparent mask as a microfluidic photomask for the soft lithography of SU-8 negative photoresist cams, which improved the manufacturing economy of soft lithography of cams. Hung et al. [29] processed a microchannel with a depth of 600 μm, and a depth ratio of 1.2 on the surface of SUS316L stainless steel by using the die micro-EDM. The material removal rate was high, while the surface roughness was 0.715 μm, and the surface quality of the microchannel was poor. This is because the EDM depends on high-frequency pulse discharge, which can form the discharge pits on the machining surface, as well as the recasting layer, resulting in the deterioration of surface quality. Micro-milling can produce micro-parts with complex three-dimensional structures at relatively low cost, high efficiency, and good surface quality [30]. Behroodi et al. [31] combined the projection micro-stereolithography (PμSL) 3D printing with computer numerical control (CNC) micro-milling method to simplify the manufacture of microfluidic devices with high-resolution microstructures. Zhang et al. [32] used the manufactured polycrystalline diamond (PCD) micro-end mill to produce the microstructure on tungsten carbide through micro-milling. However, tool wear deteriorates the machining quality in the milling process. Ultrasonic vibration has a significant impact and plays an important role in assisting different manufacturing processes [33], which can effectively reduce the processing force and tool wear in the process of micro-milling, ensuring the processing quality [34–36]. Hence, ultrasonic vibration–assisted grinding (UVAG) can be conducted to improve the surface quality and form accuracy.

Another requirement is the post-processing of the structural surface in the mould core. A variety of polishing methods, such as copying tool polishing [37], magnetic field–assisted polishing [38], and fluid jet polishing [39, 40], were conducted in recent years. The key is to improve the surface roughness without reducing the precision of the characteristic structure shape. Chemical mechanical polishing is an effective polishing method to achieve sub-nanometre surface roughness [41–43]. Nevertheless, CMP only can be utilised to machine flat surfaces. Suzuki et al. [44] used the profile-shaped diamond wheel to grind the binderless tungsten carbide Fresnel die and obtained the form accuracy of 0.8 μm in peak-to-valley (PV) value and surface roughness of 14 nm. However, it is difficult to adapt this method to the polishing of complex structures. Guo et al. [45] used the magnetic field–assisted finishing (MFAF) method to finish

the microfluidic die with a curved microstructure, reducing the surface roughness to about R_a 0.11 μm while ensuring the height of the microstructure. Kim et al. [46] polished the microstructural groove array on the silicon surface of electroplated copper by magnetorheological finishing. The surface roughness of the polished tetrahedral structure was reduced to one-tenth of the initial value, with the bottom roughness reaching 11.1 nm and the side roughness reaching 18.1 nm. Wang et al. [47] conducted a feasibility study on polishing V-groove structured surface with magnetic composite fluid slurry, and the surface roughness was reduced from 350 to 15–50 nm after 150 min of polishing. However, it is still difficult to maintain a high form accuracy with the magnetic field–assisted polishing method. Wang et al. [48] innovatively used the low-pressure fluid jet polishing method for the polishing of the sinusoidal structure surface and V-groove-structured surface without using the mask. The advantage of fluid jet polishing lies in its strong shape and material adaptability, which can be used for ultra-precision polishing of various materials [49], complex structures [50], and even inner cavities [51]. Secondly, it can ensure that the processed surface does not produce heat-affected zones [52]. Therefore, the fluid jet polishing technology is more suitable for polishing the microstructure in the microfluidic mould core surface. To enhance the polishing efficiency, multi-jet polishing technology was proposed by Wang et al. [53, 54], which can largely boost the polishing efficiency.

Based on the above introduction, most of the current studies focus on a single process in the microfluidic chip fabrication process, which makes it difficult to develop a mature fabrication process. Fewer studies focus on the large-scale fabrication process of polymeric microfluidic chips. Therefore, the process chain for low cost and mass fabrication of microfluidic chips is described in detail in this paper.

2 Methods

In this paper, the microstructure is first machined by milling and ultrasonic vibration–assisted grinding (UVAG) on the surface of the mould core using a milling cutter and ultrafine grinding tool. The key parameters of micro-grinding are studied in detail to implement the machining of the microstructure with high surface quality and form accuracy. Then, the fluid jet polishing (FJP) technology is used to improve the surface quality of the mould core of the microfluidic chip while ensuring the shape of the microstructure. Finally, the polymeric microfluidic chip is efficiently fabricated by replicating the microstructure on the mould core surface to the polymer surface using microinjection moulding technology. Figure 1 shows the complete process chain for the mass production of polymeric microfluidic chips.

3 Experiments

3.1 Mould core material

The machining performance of mould steel is better than materials with high hardness such as ceramics and hard

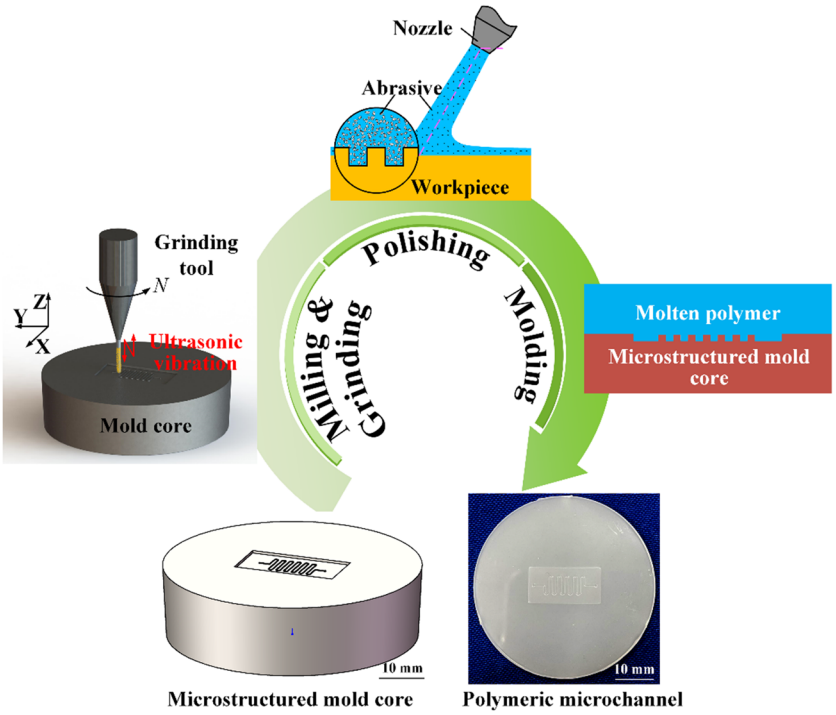

Fig. 1 Process chain for the mass production of polymeric microfluidic chips

alloys. Therefore, the mould core material is mould steel S136H. Its material properties are shown in Table 1, the mould steel has excellent corrosion resistance, wear resistance, and good machining and polishing performance.

3.2 Experimental detail

3.2.1 Milling and grinding process of the microstructural mould core

To reduce the machining allowance of micro-milling and prolong the service life of micro-grinding rod tools, the machining process of the microstructural mould core can be divided into three steps. The first step is to use a carbide milling tool with a diameter of 1 mm to rough mill the mould to generate the micro-convex structure outline. In the second step, a carbide milling tool with a diameter of 0.5 mm was used to conduct semi-finish milling to improve the surface quality. In the third step, a cubic boron nitride (CBN) grinding tool with a grain size of #800 and a diameter of 0.3 mm (Resmo, Japan) was used to perform UVAG, and a microstructural mould core with high form accuracy and surface quality was produced, as shown in Fig. 2. The workpiece is not disassembled during the processing to avoid installation error, and only the length compensation of the grinding bar is needed. The process is carried out on the precision three-axis machining centre to complete the length compensation of the fine grinding bar to ensure the accuracy of the tool.

The UVAG experiment was carried out on the three-axis ultrasonic machining centre (UHB-500), as shown in Fig. 3. The vibration frequency is 25–35 kHz with an amplitude of 4 μm. The fine-grained CBN electroplating grinding tool was used in the UVAG process experiment. To obtain the influence of different process parameters on grinding quality and realize the optimization of the UVAG process, the influences of grinding process parameters including spindle speed N, feed speed v_f, grinding depth a_p, and ultrasonic power P_a on the surface quality of microstructure machining were studied. Detailed processing parameters are shown in Table 2.

For the testing experiments in FJP, the design of the workpiece is simplified and scaled down. The surface roughness R_a of the top surface of the raised microstructure is between 0.182 and 0.199 μm, and the surface roughness of the bottom surface of the microstructure is between 0.481 and 0.503 μm.

Table 1 Material properties of S136H

Properties	Value
Hardness (HRC)	50
Density (kg/m^3)	7800
Modulus of elasticity (MPa)	200,000
Tensile strength (N/mm^2)	1780
Yield strength (N/mm^2)	1360

3.2.2 Fluid jet polishing (FJP) of the microstructural mould core

The ZEEKO IRP200 polishing machine was selected for the fluid jet polishing experiment, which has a 7-axis polishing system equipped with a sapphire nozzle, as shown in Fig. 4a. In FJP, the polishing slurry containing water and abrasive is pressurised and pumped out of the nozzle to generate the fluid jet, and the fluid jet impinges the target surface to generate the micro-/nanometre scale material removal induced by the erosion of the high-speed abrasive in the slurry, as shown in Fig. 4b. Because it adopts the flexible jet as the carrier, FJP has a high adaptability to the surface with complex and irregular structures. The polishing slurry used in

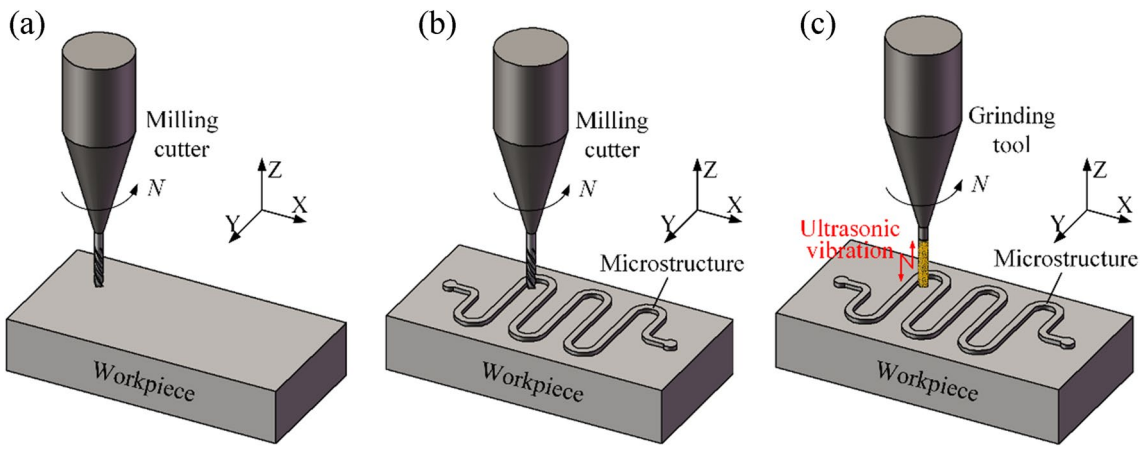

Fig. 2 Schematic diagram of mould core machining process: **a** rough milling, **b** semi-finish milling, and **c** fine grinding

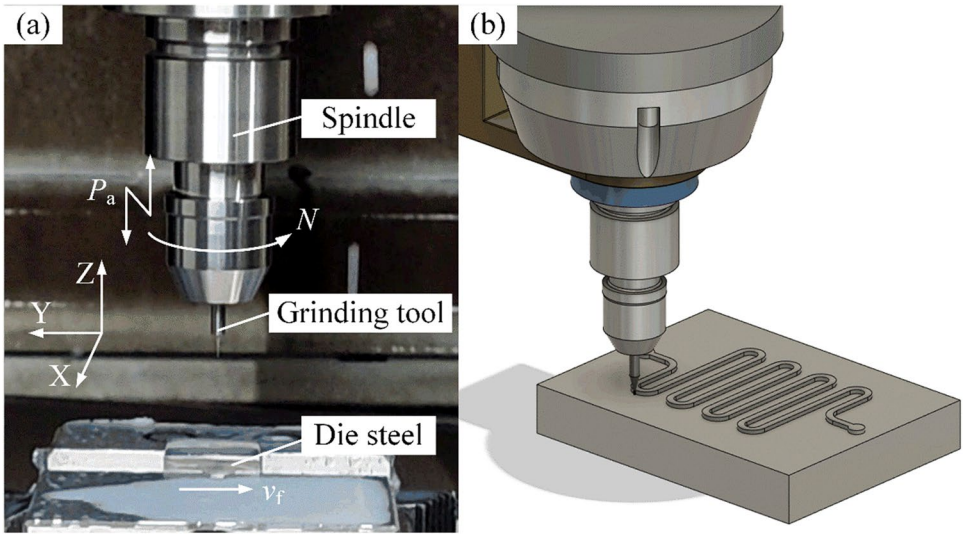

Fig. 3 Experimental setup of ultrasonic vibration grinding machining centre: **a** machining picture and **b** machining diagram

Table 2 Experimental parameters of ultrasonic vibration–assisted grinding of mould steel

Spindle speed N (r/min)	Feed rate v_f (mm/min)	Grinding depth a_p (μm)	Power P_a (%)
18,000	15	3	90
22,000	15	3	90
26,000	15	3	90
30,000	15	3	90
30,000	5	3	90
30,000	25	3	90
30,000	35	3	90
30,000	15	1	90
30,000	15	2	90
30,000	15	4	90
30,000	15	3	70
30,000	15	3	50
30,000	15	3	30

the experiment was silicon carbide abrasive (GC #1000, Fujimi) with a concentration of 6 wt.% and an average abrasive radius of 11.9 μm. The effect of some critical parameters in FJP is investigated, including the feed speed, fluid pressure, impinging angle, and stand-off distance. Table 3 shows the detailed experimental conditions of the polishing process.

3.2.3 Microinjection moulding of polymeric microfluidic chip

BABYPLAST 6/10P injection moulding machine was selected for the microinjection moulding process of the microfluidic chip, as shown in Fig. 5a. The principle of injection moulding is shown in Fig. 5b. Polymer particles flow into the plasticizing chamber through the hopper, melt at high temperature, and then inject into the mould cavity with micro-raised array structure mould core through the

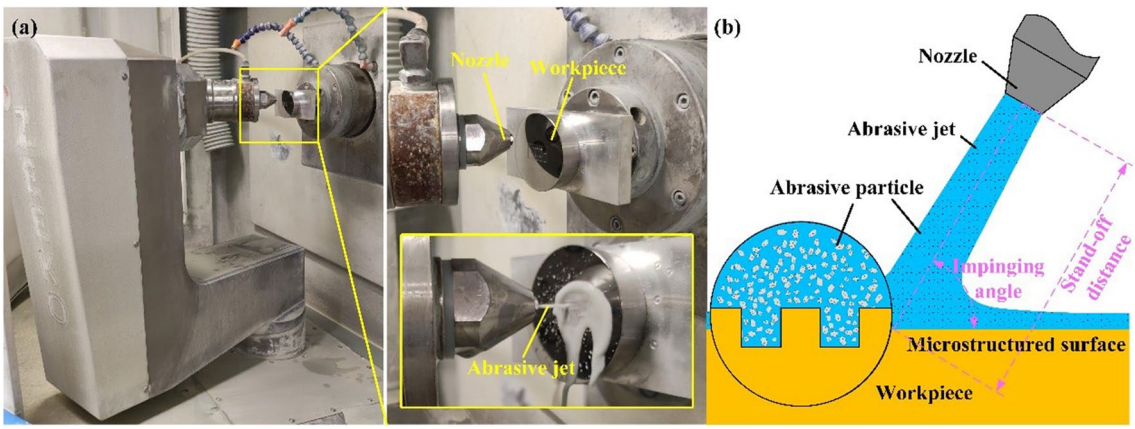

Fig. 4 Experimental setup and the principle of fluid jet polishing. **a** Photograph of the experimental setup. (**b**) Schematic diagram

Table 3 Experimental parameters of fluid jet polishing process for mould core

	Feed rate F (mm/min)	Fluid pressure P (bar)	Impinging angle A (°)	Stand-off distance T (mm)
1	10	8	90	4
2	30	8	90	4
3	50	8	90	4
4	70	8	90	4
5	30	6	90	4
6	30	8	90	4
7	30	10	90	4
8	30	12	90	4
9	30	8	45	4
10	30	8	60	4
11	30	8	75	4
12	30	8	90	4
13	30	8	90	2
14	30	8	90	4
15	30	8	90	6
16	30	8	90	8

gate. After the pressure holding and cooling stage, the pattern on the microchannel mould core was transferred to the polymer and solidified. Finally, the polymer sample was pushed out by the thimble after the front and back mould separation, to achieve the purpose of polymer microfluidic chip scale replication forming. The selected material was polypropylene (PP, LG B310), which possesses excellent heat resistance, bending fatigue resistance, and corrosion resistance. It is widely used in microinjection moulding of polymer microfluidic chips. In this experiment, the influence of key injection process parameters such as melt temperature, injection speed, holding pressure, and holding time on the surface quality and form accuracy of polymeric microchannel was studied. Table 4 shows the experimental parameters of the microinjection moulding process.

3.3 Measurement and characterisation methods

3D surface profiler (Keyence VK-X260) was used to measure the processed surface of mould steel by UVAG. The surface roughness of mould steel was obtained according to the measured 3D topography, and the average value of 10 measured data was selected as the roughness R_a. The surface roughness (S_a) and morphologies of the bottom surface of the microstructural mould core were measured by using a white light interferometer (ZYGO Nexview) and scanning electron microscope (SEM). The mean values of two different areas on the underside of the microstructure for each polishing parameter during measurement were selected.

The roughness at the bottom of the polymer microchannel structure was measured by a stylus profiler (KLA-Tencor D-300). Five sample lengths were selected from the bottom profile of the polymer microfluidic chip to calculate the roughness at the bottom of the flow channel, and their average value was taken as the roughness value R_a of the bottom surface of the polymeric microfluidic chip. The form of the convex microstructure was measured by a non-contact 3D laser confocal microscope (Keyence VK-X260). The micro-convex structure was designed with a 6° structural slope to facilitate the demolding of the injection moulding workpiece.

4 Results and discussions

4.1 Precision ground surface of the microstructural mould core

Figure 6 shows the surface roughness R_a of the mould steel under different ultrasonic vibration–assisted grinding process parameters. It can be seen that the surface roughness R_a gradually decreases with the increase of spindle speed as shown in Fig. 6a. This is induced by that the effective abrasive grains involved in grinding per unit of time

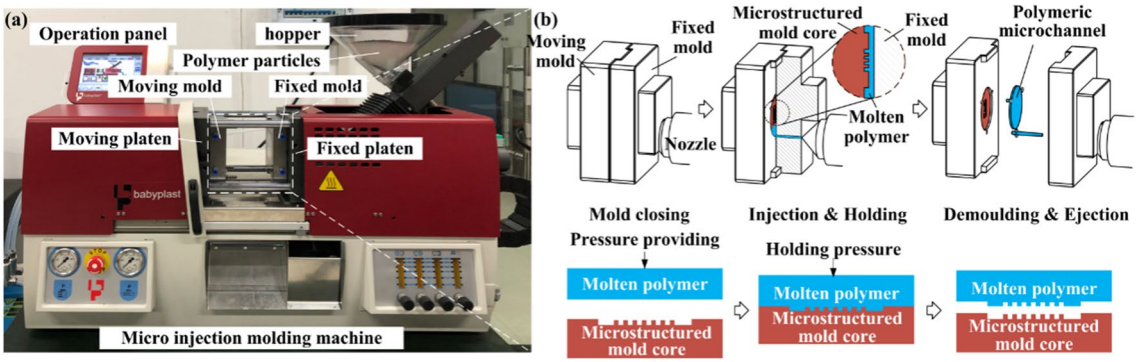

Fig. 5 Experimental setup and the principle of the microinjection process. **a** Photograph of the experimental setup. **b** Schematic diagram of microinjection moulding process

Table 4 Experimental parameters of the microinjection process

	Melt temperature T (℃)	Injection speed V (mm/s)	Holding pressure P (MPa)	Holding time t (s)
1	205	80	5	5
2	215	80	5	5
3	225	80	5	5
4	235	80	5	5
5	245	80	5	5
6	235	40	5	5
7	235	50	5	5
8	235	60	5	5
9	235	70	5	5
10	235	80	3	5
11	235	80	4	5
12	235	80	6	5
13	235	80	7	5
14	235	80	5	1
15	235	80	5	3
16	235	80	5	7
17	235	80	5	9

gradually increase, resulting in an effective improvement of the machined surface quality. There is no increase in surface roughness due to the excessive wear of abrasive grains at higher rotational speeds. It indicates that even when using smaller abrasive grains for machining mould steel, the ultrasonic vibration–assisted machining technology is invoked to effectively reduce the abrasive grain wear and maintain the sharpness of abrasive grains at higher rotational speeds. As can be seen from Fig. 6b, with the increase in the feed rate, the roughness of the machined surface of mould steel presents a rising trend. When the feed rate is 5 mm/min, the surface roughness R_a reaches the lowest value of 0.195 µm. Since the experiments were conducted with grinding rods having a finer grit, the lower feed rates contributed to effective material removal and improved surface quality. As shown in Fig. 6c, the machined surface roughness decreases with the increase of the cutting depth when the cutting depth is less than 2 µm and increases when the cutting depth a_p exceeds 2 µm. The main reason for this phenomenon is the 'ploughing phenomenon' when the cutting depth a_p is lower [55]. The material flow sideways when the abrasive particles squeeze the workpiece surface, reducing the grinding surface quality. Figure 6d shows the relationship between the ultrasonic power and the processed surface quality of mould steel. With the increase of ultrasonic power, the surface roughness first decreases and then increases. When the ultrasonic power is 70%, the machined surface roughness of mould steel reaches a small value of 0.303 µm. In conclusion, the machined surface roughness R_a of mould steel varies from 0.195 to 0.458 µm under different grinding processes. When the spindle speed N, feed rate v_f, cutting depth a_p, and ultrasonic power P_a are 30,000 r/min, 5 mm/min, 2 µm, and 90%, respectively, the machining quality is better.

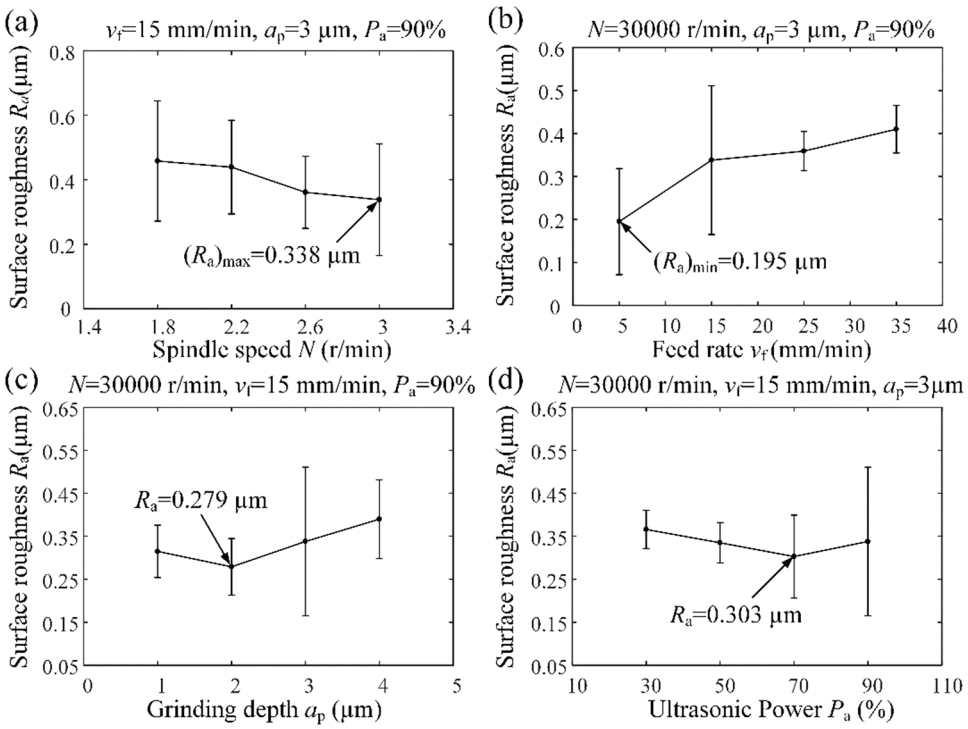

Fig. 6 Influences of ultrasonic vibration–assisted grinding process parameters on surface quality: **a** spindle speed N, **b** feed rate v_f, **c** grinding depth a_p, and **d** ultrasonic power P_a

Figure 7 shows the macroscopical picture and overall 3D morphology of the micromachined mould core with a micro-convex array structure. It can be seen from the figure that the microstructure processed by UVAG has a clear overall outline and smooth surface, which achieves higher sidewall verticality and higher processing quality. According to the inspection data, the bottom roughness R_a of the micro-convex structure is about 0.346 μm, the top roughness R_a of the micro-convex structure is about 0.136 μm, the average width of the microstructure is 237.352 μm, and the average height is 168.407 μm.

4.2 Precision polished surface of the microstructural mould core

Figure 8 shows the SEM photographs of the microstructure. Figure 9 shows the surface morphologies and surface roughness of the mould after polishing under different conditions. The colour represents the surface height at different positions. The results of the 3D surface roughness results have been summarised in Fig. 10. As shown in Fig. 10a, the influence of the feed rate on the polished surface quality is demonstrated, with the range of surface roughness variation in surface mean height (S_a) from 0.063 to 0.049 μm. Figure 8a shows the surface morphology of the mould core under different feed rates. Surface roughness S_a tends to decrease and then increase with increasing feed rate. At a lower feed rate, more material is removed from the surface of the microstructure even after the grinding marks are removed. Larger polishing grains produce more processing marks on the surface, resulting in poor polishing quality and uniformity. In addition, excessive material removal can destroy the integrity of the microstructure boundary and even change the microstructure contour. As shown in Fig. 8a, when the feed rate is lower than 50 mm/min, the shape of the microstructure contour changes greatly. Especially when the feed rate is at 10 mm/min, the width of the microstructure is greatly reduced due to the high material removal per unit time. When the feed rate is increased to 50 mm/min, microstructure surface quality is better, indicating that the surface machining marks can be removed well at this time. Under this condition, the edges of the microstructure are clear, and the machining marks are not obvious. Meanwhile, there is no obvious form change. Therefore, the form accuracy of the microstructure can be guaranteed, and the polishing quality is the best, as shown in Fig. 8a. The polished surface quality decreases again after 50 mm/min. In Fig. 8a, the feed rate F larger than 50 mm/min shows no significant change in the microstructure either, indicating that the material removal per unit time of the fluid jet decreases with the continuous increase of feed rate. This results in the inability to completely remove the marks produced by milling and grinding.

Figure 10b shows the influence of the fluid pressures on polished surface quality. With the increase in fluid pressure, the average surface roughness S_a at the bottom decreases first and then increases, with a range of 0.077 ~ 0.061 μm. Figure 8b shows the surface topography of the mould core under different fluid pressures. Fluid pressure mainly affects the impact velocity of the abrasive fluid in the process of FJP, which can have a significant impact on polishing performance. According to Fig. 10b, the surface roughness is 0.061 μm when the fluid pressure is 8 bar. When the fluid pressure is less than 8 bar, the impact velocity decreases, and the number of abrasive particles per unit of time also decreases. This limits the material removal rate per unit of time, resulting in inadequate polishing and poor surface quality. In this situation, no significant deformation is found in the morphology of the microstructure mould core when the fluid pressure is 6 bar or 8 bar as shown in Fig. 10b. When the fluid pressure is greater than 8 bar, more abrasive particles per unit of time participate in the polishing process together with higher energy per particle, resulting

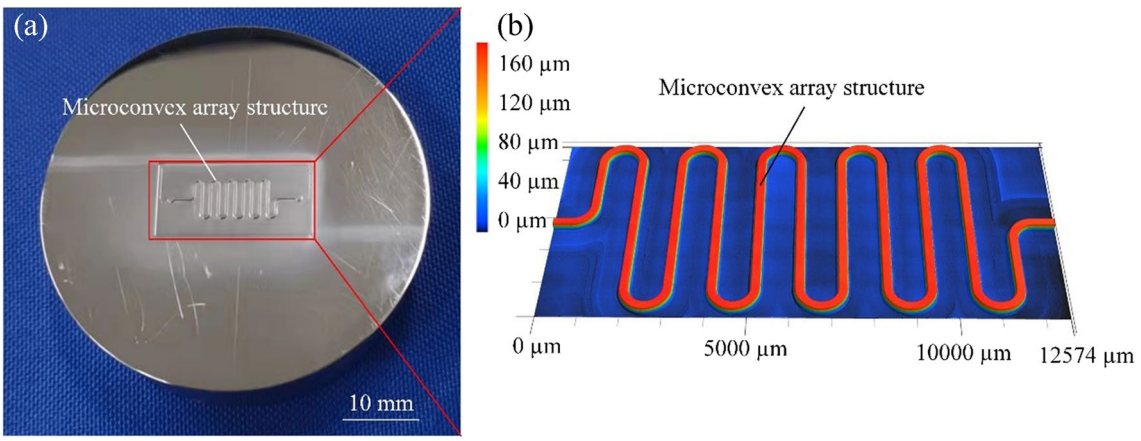

Fig. 7 Photo and 3D morphology of micro-convex array structured mould core: **a** macroscopical picture and **b** 3D morphology

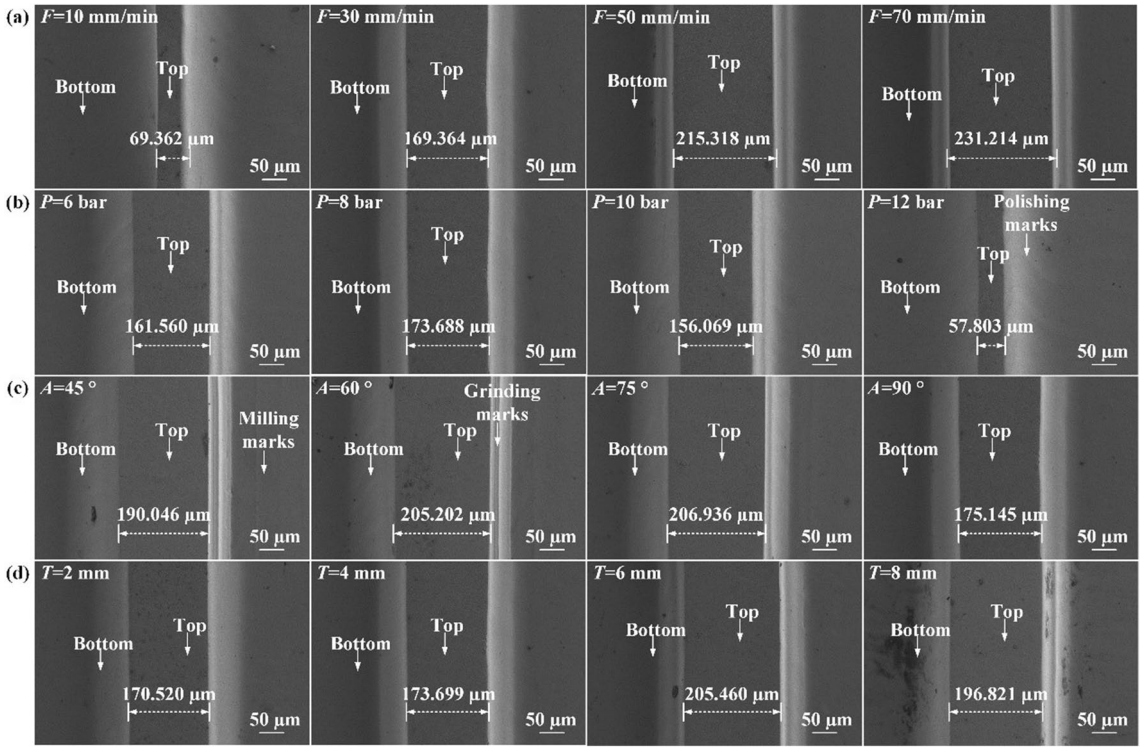

Fig. 8 SEM images of microstructure under different polishing process parameters: **a** feed rate F, **b** fluid pressure P, **c** impinging angle A, and **d** stand-off distance T

in excessive material removal of abrasive particles. Higher impact velocity leads to deeper indentation of abrasive particles on the polished surface, resulting in higher surface roughness, especially when the fluid pressure reaches 12 bar. According to Fig. 8b, it is noted that the microstructure also has large shape changes, indicating that excessive polishing occurs.

Impinging angle reflects the angles between the fluid jet and the target surface in the process of machining. Different impinging angles will affect the direction of abrasive particles impacting the target surface material, which is an important factor in the FJP process. Figure 10c shows the influence of different impinging angles on the polished surface quality. While Fig. 8c shows the changes in the surface morphology of the mould core at different impinging angles. With the increasing impinging angle, the average surface roughness S_a at the bottom rises first, then decreases, and tends to be stable, with a range of 0.063 ~ 0.050 μm. As can be seen from Fig. 8c, when the impinging angle is 45°, the surface quality is best, and the average surface roughness S_a is 0.050 μm. However, according to the surface topography, the inconsistency of polishing quality appeared on both sides of the microstructure, which affects the polishing quality. When the impinging angle is 90°, over-polishing occurs due to excessive material removal, which not only seriously affects the surface quality, but also seriously damages the form accuracy. Therefore, a larger impinging angle is easy to adversely affect the surface roughness and form accuracy. Hence, a smaller impinging angle should be selected in the process of FJP to obtain better surface quality.

Stand-off distance reflects the distance between the nozzle and the target surface, which is also an important parameter in FJP. Figure 10d shows the influence of the stand-off distance on polished surface quality, and Fig. 8d shows the surface topography of the mould core under different stand-off distances. No obvious relationship between the surface roughness and the stand-off distance is found in this study, which means that the effect of the stand-off distance on the surface roughness is not obvious. This phenomenon is consistent with the reference [56].

In summary, the optimised polishing process parameters are feed rate $F = 50$ mm/min, fluid pressure $P = 8$ bar, impinging angle $A = 45°$, and stand-off distance $T = 4$ mm. The results show that the FJP technology can be used to polish the microstructure of complex microchannel mould cores. The surface quality of the microchannel mould core was improved greatly after FJP based on the optimised polishing process parameters. Figure 11a, c demonstrates the 3D topography of the microstructure before and after polishing, respectively. And Fig. 11b, d presents the SEM photographs of the microfluidic mould core before and after polishing. It can be seen from Fig. 11b that there are

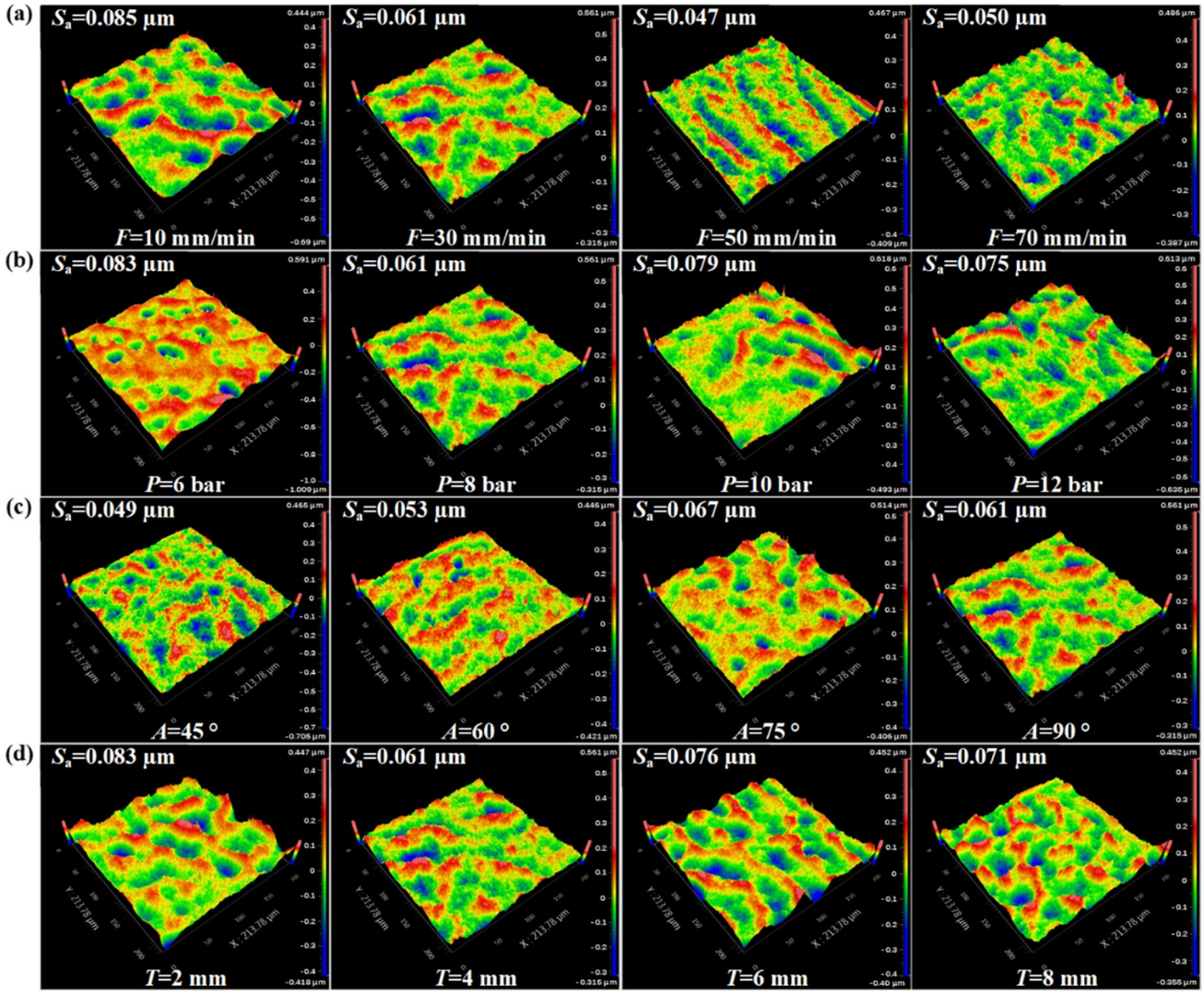

Fig. 9 3D topographies at the bottom of the microstructure under different polishing process parameters: **a** feed rate *F*, **b** fluid pressure *P*, **c** impinging angle *A*, and **d** stand-off distance *T*

burrs on the edge of the side wall of the microstructure before polishing, as well as obvious milling and grinding marks. After FJP, the surface has been improved by removing the burrs and milling/grinding marks on the side wall. The average surface roughness of the microstructure is S_a 0.051 μm at the top and 0.230 μm at the bottom. The results show that FJP can significantly improve the surface quality of the microstructure.

As shown in Fig. 12a, the height deviation *e* of the two curves can be obtained by comparing the section profile of the mould core micro-convex structure with that of the theoretical machined section. The PV value of the deviation curve can be used to calculate the form accuracy of microstructural mould core The form deviation PV value of the machined mould core with a micro-convex structure can be calculated as 15.681 μm by the PV value of the height deviation curve, as shown in Fig. 12b.

4.3 Microinjection moulding quality of polymeric microchannel

Figure 13 shows the influence of different injection process parameters on the roughness R_a at the bottom of the polymeric microchannel. Overall, melt temperature *T* and holding time *t* have more significant effects on the roughness R_a at the bottom of the polymeric microchannel. Figure 13a reflects that the roughness at the bottom of the microchannel decreases with the increase in melt temperature. When the melt temperature increases to 245 °C, the roughness R_a at the bottom of the microchannel can reach a minimum value of

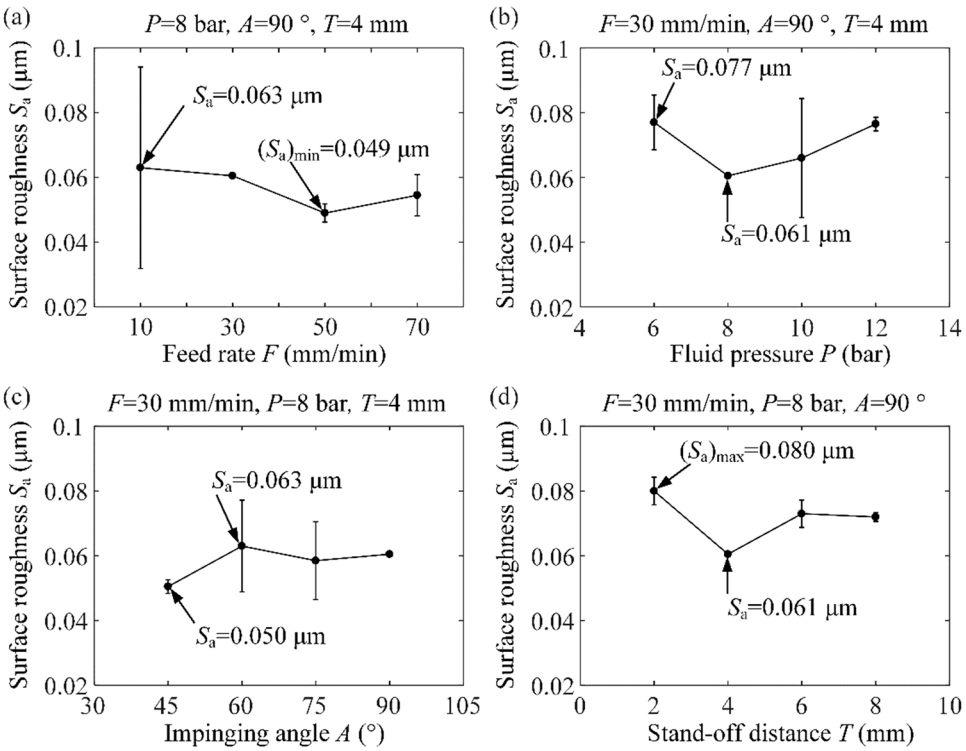

Fig. 10 Effects of polishing process parameters on surface quality: **a** feed rate *F*, **b** fluid pressure *P*, **c** impinging angle *A*, and **d** stand-off distance *T*

0.029 μm. Figure 13b shows that with the increase of injection velocity *V*, the roughness of polymer microinjection presents a slight downward trend. The main reason is that the structural changes caused by the microstructure's protrusion side walls and rounded corners at the bottom make the microinjection moulding filling process more difficult. The faster injection speed allows the molten polymer to fill the cavity more quickly, reducing the effect of too fast temperature drop. It can be seen from Fig. 13c that the roughness R_a at the bottom of the micro-flow channel changes not significantly with the increase of the holding pressure *P*, ranging from 0.033 to 0.030 μm. When the holding pressure exceeds 5 MPa, the surface roughness of the workpiece increases. As can be seen from Fig. 13d, the roughness R_a at the bottom of the micro-flow channel gradually decreases with the increase of the holding time *T*. When the holding time exceeds 5 s, the roughness at the bottom of the polymeric microchannel increases slightly and then reaches 0.027 μm when the holding time reaches 9 s.

Figure 14 reflects the different microinjection moulding process parameters on the form accuracy PV of the polymeric microchannel. The polymeric microchannel still maintains a high form accuracy when the mould core microstructure has a higher perpendicularity and the fillet radius is smaller. With the change of moulding process parameters, the form accuracy of the polymeric microchannel ranged from 8.594 to 16.180 μm. Melting temperature and holding time have a great influence on form accuracy. As shown in Fig. 14a, the form accuracy PV of polymer injection parts decreases sharply at first and then tends to be stable with the increase of melt temperature *T*. This is because the low melt temperature makes the polymer melt flow insufficient, resulting in insufficient filling of injection parts and affecting the form accuracy of the polymeric chip. As can be seen from Fig. 14b, the form accuracy PV of polymeric microchannel rises slowly first and then decreases slightly with the increase of injection velocity *V*. As shown in Fig. 14c, the form accuracy PV of microchannel maintains at a stable level with the increase of holding pressure *P*. As shown in Fig. 14d, the form accuracy PV of the microchannel decreases sharply first and then slowly with the increase of the holding time *T*. When the holding time is 9 s, melt temperature is 235 °C, injection speed is 80 mm/s, and holding pressure is 5 MPa, the form accuracy PV of the microchannel reaches a minimum value of 8.594 μm, and the roughness R_a of the microchannel at the bottom is 0.027 μm. The microstructure characteristics of polymer chips processed by UVAG have higher surface quality and form accuracy.

Figure 15 shows the photograph and morphology of the polymeric microchannel when the melt temperature is 235 ℃, the injection speed is 80 mm/s, the pressure holding pressure is 5 MPa, and the pressure holding time is 8 s. Figure 15a shows the macroscopic photograph of the polymeric microfluidic chip. Figure 15b, c shows the 3D morphologies of the polymeric microfluidic chip and microchannel, respectively. The side wall of the microchannel has high verticality and clear and complete boundary due to high injection moulding accuracy. In Fig. 15d, e, the SEM images of the

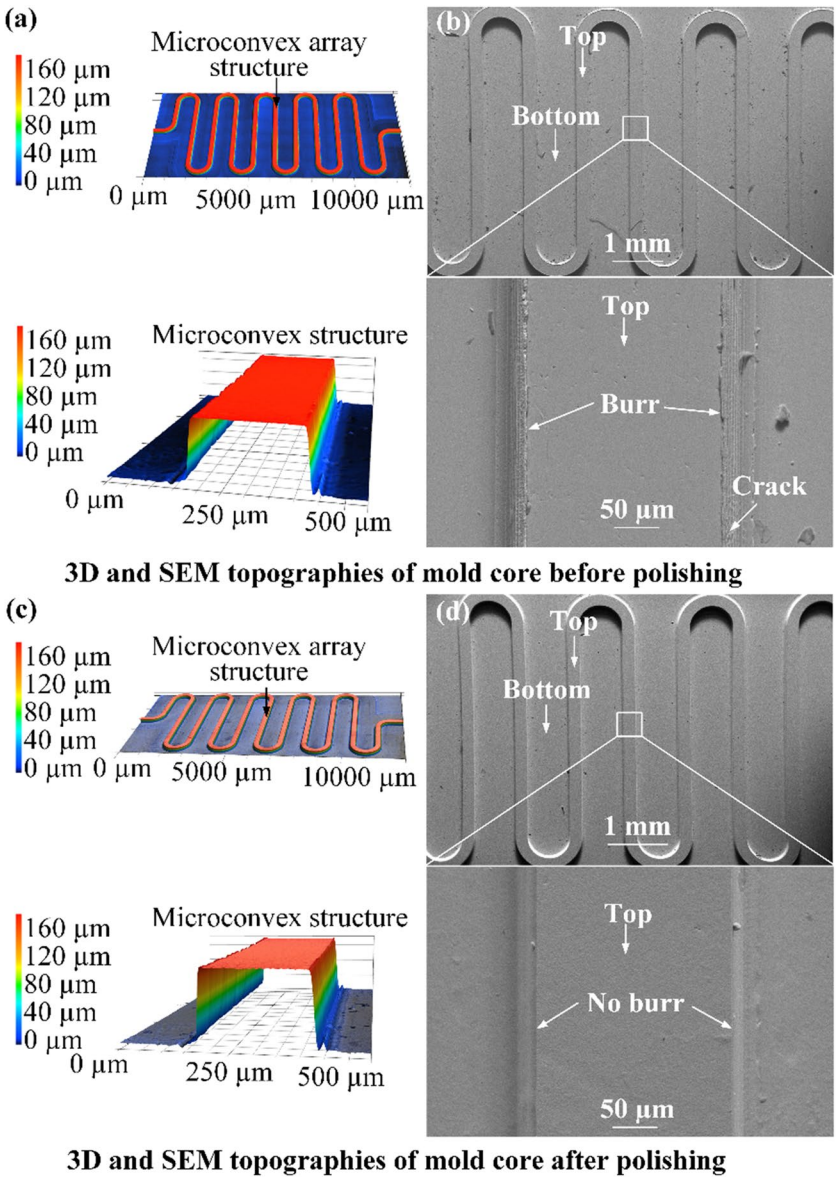

Fig. 11 3D morphology and SEM images of mould core before and after polishing: **a** 3D morphology before polishing, **b** SEM images before polishing, **c** 3D morphology after polishing, and **d** SEM images after polishing

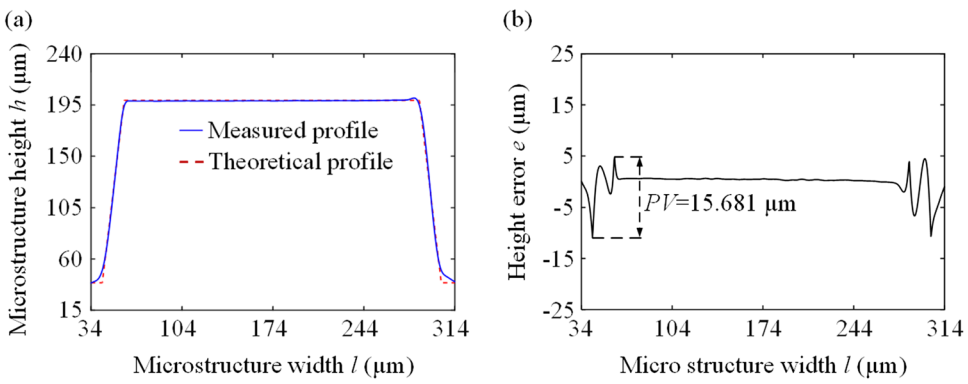

Fig. 12 **a** Section profile curves of theoretical and machined microstructural mould core. **b** Form accuracy of microstructural mould core

polymeric microfluidic chip and microchannel can be seen, respectively. The surface at the top and bottom of the microchannel is very smooth. The bottom surface roughness R_a is 0.027 μm. The structure and the edge of the microchannel have no obvious shrinkage and flow marks or other defects. The microinjection moulding quality is considerably high.

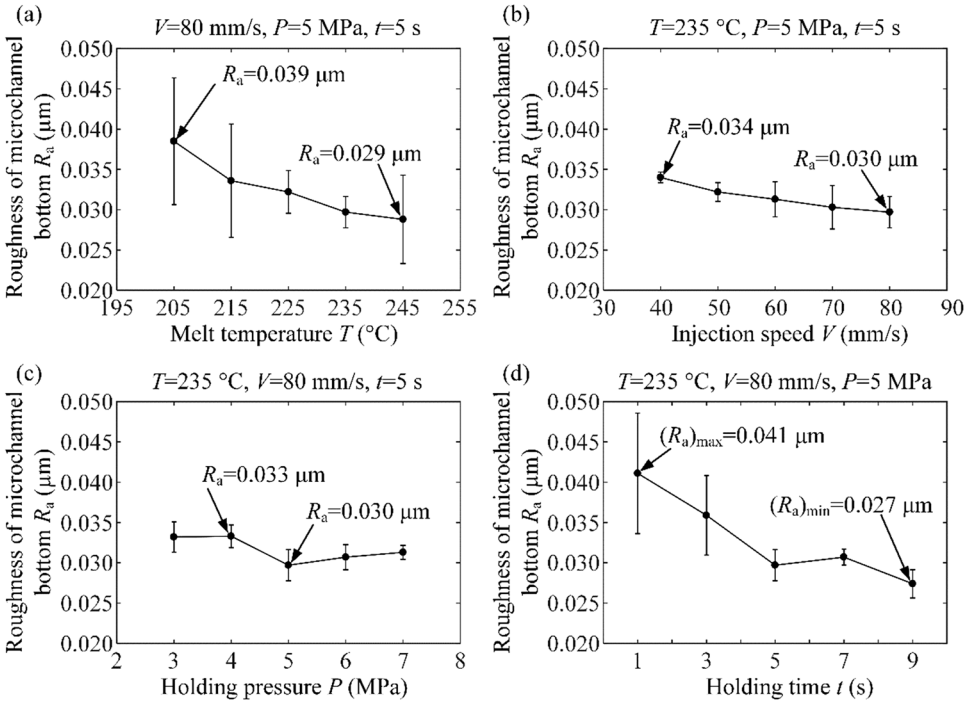

Fig. 13 Influences of microinjection process parameters on the roughness of microchannel bottom: **a** melt temperature *T*, **b** injection speed *V*, **c** holding pressure *P*, and **d** holding pressure *t*

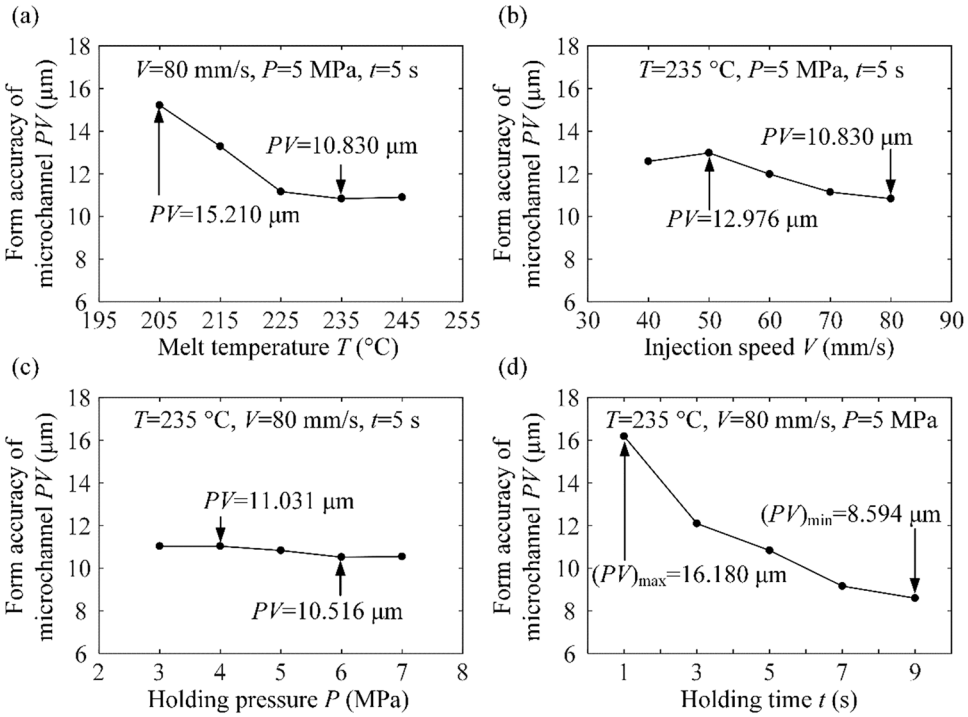

Fig. 14 Influences of microinjection process parameters on form accuracy PV of polymeric microchannel: **a** melt temperature *T*, **b** injection speed *V*, **c** holding pressure *P*, and **d** holding pressure *t*

The section profile of the micro-convex structure of the mould core was compared with that of the polymeric microchannel, and the former was obtained along the direction *h* of the mould core micro-convex height, as shown in Fig. 16a. The height deviation *e* is obtained by the difference between the two curves, and the PV value of the deviation curve can be used to calculate the form

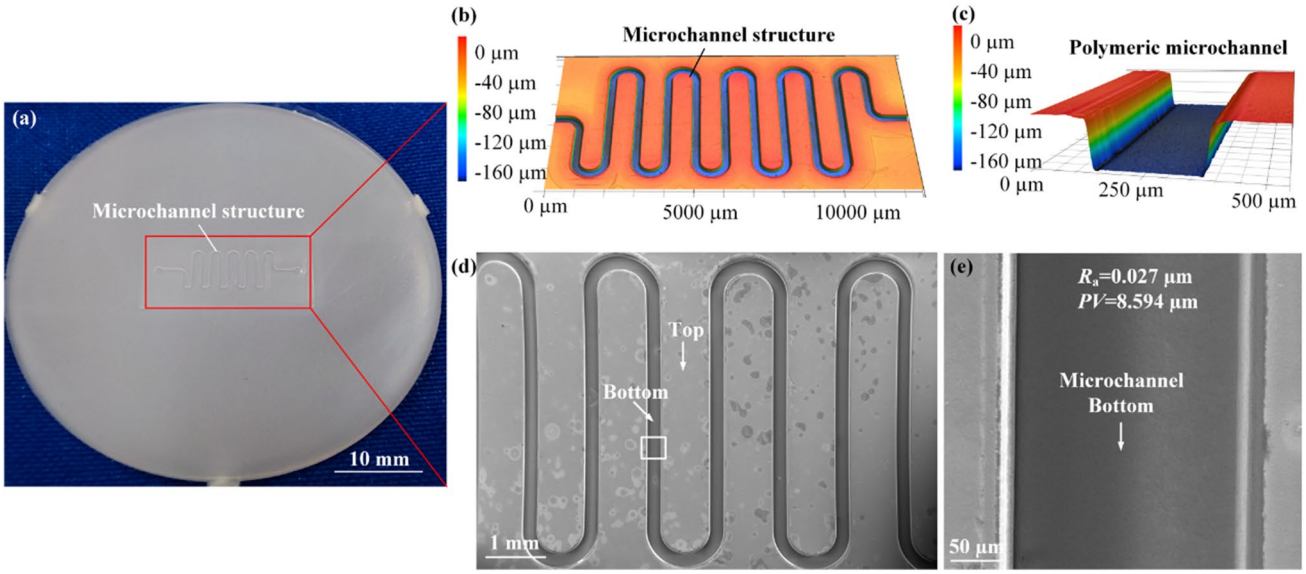

Fig. 15 **a** Photograph of the polymeric microfluidic chip; **b** 3D topography of polymeric microfluidic chip; **c** 3D topography of polymeric microchannel; **d** SEM image of polymeric microfluidic chip; **e** SEM image of polymeric microchannel

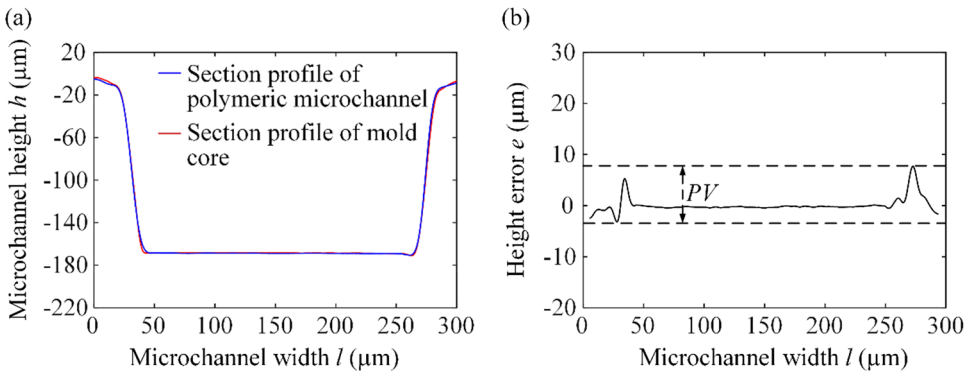

Fig. 16 **a** Section profiles of microstructural mould core and polymeric microchannel. **b** Form accuracy of polymeric microchannel by injection moulding

accuracy of the polymeric microchannel structure, as shown in Fig. 16b.

5 Conclusions

In this paper, a process chain of microfluidic chips including milling, ultrasonic vibration–assisted grinding (UVAG), fluid jet polishing (FJP), and injection moulding is introduced in detail, which can not only realize low cost and mass production of the polymeric microfluidic chips but also reduce energy consumption. The processing parameters of UVAG, FJP, and injection moulding were optimised and systematically analysed based on the form accuracy and surface quality. The main research results and conclusions are as follows:

(1) UVAG and FJP can be combined to realize the precision machining of the mould core for the microfluidic chips with controllable form accuracy and surface quality.

(2) In UVAG of the mould steel, the surface roughness decreases with the increase of spindle speed and increases with the increase of feed rate. In addition, the roughness decreases first and then increases with the increase of cutting depth and ultrasonic power.

(3) In the FJP of the mould core, the surface roughness S_a firstly decreases and then increases with the increase in feed rate and fluid pressure. The roughness increases first, then decreases, and tends to be stable with the increase in injection angle. There is no obvious relationship between the stand-off distance and the surface roughness. It was found that the FJP is effective

to remove the debris and grinding marks left on the channel surface, improving the surface quality.

(4) In the microinjection process of the polymer chips, the surface roughness and form accuracy of the microchannel decrease with the increase of melt temperature and holding time, while the effect of injection speed and holding pressure is gentle. The form accuracy of the microchannel reaches 8.594 μm, and the roughness of the microchannel is 0.027 μm.

Author contribution All authors contributed to the study's conception and design. Material preparation, data collection, and analysis were performed by Yanjun Lu, Bo Liu, and Zili Zhang. The first draft of the manuscript was written by Yanjun Lu, and all authors commented on previous versions of the manuscript. All authors read and approved the final manuscript.

Funding The work described in this paper was mainly supported by the National Natural Science Foundation of China (No. 51805334), the International Science and Technology Cooperation Project of Shenzhen City (No. GJHZ20190822091805371), the Guangdong Natural Science Foundation Program 2019–2020 (No. 2019A1515012015), and the Shenzhen-Hong Kong-Macau Technology Research Programme (Project No: SGDX20220530110804030).

Declarations

Ethics approval Not applicable.

Consent to participate Not applicable.

Consent for publication Not applicable.

Competing interests The authors declare no competing interests.

References

1. Berlanda SF, Breitfeld M, Dietsche CL, Dittrich PS (2021) Recent advances in microfluidic technology for bioanalysis and diagnostics. Anal Chem 93:311–331. https://doi.org/10.1021/acs.analchem.0c04366
2. Kimura H, Sakai Y, Fujii T (2018) Organ/body-on-a-chip based on microfluidic technology for drug discovery. Drug Metab Pharmacokinet 33:43–48. https://doi.org/10.1016/j.dmpk.2017.11.003
3. He S, Joseph N, Feng S et al (2020) Application of microfluidic technology in food processing. Food Funct 11:5726–5737. https://doi.org/10.1039/D0FO01278E
4. Wang H, Zhao K, Shen H, Yao Z (2020) Experimental study on direct fabrication of micro channel on fused silica by picosecond laser. J Manuf Process 55:87–95. https://doi.org/10.1016/j.jmapro.2020.03.057
5. He F, Liao Y, Lin J et al (2014) Femtosecond laser fabrication of monolithically integrated microfluidic sensors in glass. Sensors 14:19402–19440. https://doi.org/10.3390/s141019402
6. Peng Y, Jiang S, Xia L et al (2020) Direct ink writing combined with metal-assisted chemical etching of microchannels for the microfluidic system applications. Sens Actuators Phys 315:112320. https://doi.org/10.1016/j.sna.2020.112320
7. Wang T, Chen J, Zhou T, Song L (2018) Fabricating microstructures on glass for microfluidic chips by glass molding process. Micromachines 9:269. https://doi.org/10.3390/mi9060269
8. Ku X, Zhang Z, Liu X et al (2018) Low-cost rapid prototyping of glass microfluidic devices using a micromilling technique. Microfluid Nanofluidics 22:1–8. https://doi.org/10.1007/s10404-018-2104-y
9. Ren K, Zhou J, Wu H (2013) Materials for microfluidic chip fabrication. Acc Chem Res 46:2396–2406. https://doi.org/10.1021/ar300314s
10. Vasilescu SA, Bazaz SR, Jin D et al (2020) 3D printing enables the rapid prototyping of modular microfluidic devices for particle conjugation. Appl Mater Today 20:100726. https://doi.org/10.1016/j.apmt.2020.100726
11. Xu J, Su Q, Shan D, Guo B (2019) Sustainable micro-manufacturing of superhydrophobic surface on ultrafine-grained pure aluminum substrate combining micro-embossing and surface modification. J Clean Prod 232:705–712. https://doi.org/10.1016/j.jclepro.2019.05.394
12. Guan B, Cherrill M, Pai J-H, Priest C (2019) Effect of mould roughness on injection moulded poly (methyl methacrylate) surfaces: roughness and wettability. J Manuf Process 48:313–319. https://doi.org/10.1016/j.jmapro.2019.10.024
13. Tiboni M, Tiboni M, Pierro A et al (2021) Microfluidics for nanomedicines manufacturing: an affordable and low-cost 3D printing approach. Int J Pharm 599:120464. https://doi.org/10.1016/j.ijpharm.2021.120464
14. Xu J, Wang K, Sheng H et al (2020) Energy efficiency optimization for ecological 3D printing based on adaptive multi-layer customization. J Clean Prod 245:118826. https://doi.org/10.1016/j.jclepro.2019.118826
15. Waldbaur A, Rapp H, Länge K, Rapp BE (2011) Let there be chip—towards rapid prototyping of microfluidic devices: one-step manufacturing processes. Anal Methods 3:2681–2716. https://doi.org/10.1039/C1AY05253E
16. Lin T-Y, Do T, Kwon P, Lillehoj PB (2017) 3D printed metal molds for hot embossing plastic microfluidic devices. Lab Chip 17:241–247. https://doi.org/10.1039/C6LC01430E
17. Trotta G, Volpe A, Ancona A, Fassi I (2018) Flexible micro manufacturing platform for the fabrication of PMMA microfluidic devices. J Manuf Process 35:107–117. https://doi.org/10.1016/j.jmapro.2018.07.030
18. Albero J, Nieradko L, Gorecki C et al (2009) Fabrication of spherical microlenses by a combination of isotropic wet etching of silicon and molding techniques. Opt Express 17:6283–6292. https://doi.org/10.1364/OE.17.006283
19. Wang J, Wang H, Lai L, Li Y (2021) Preparation of microneedle array mold based on MEMS lithography technology. Micromachines 12:23. https://doi.org/10.3390/mi12010023
20. Wu X, Liu Y, Zhang X et al (2020) Sustainable and high-efficiency green electrical discharge machining milling method. J Clean Prod 274:123040. https://doi.org/10.1016/j.jclepro.2020.123040
21. Jiang K, Wu X, Lei J et al (2021) Investigation on the geometric evolution of microstructures in EDM with a composite laminated electrode. J Clean Prod 298:126765. https://doi.org/10.1016/j.jclepro.2021.126765
22. Davoudinejad A, Li D, Zhang Y, Tosello G (2020) Effect of progressive tool wear on the functional performance of micro milling process of injection molding tool. Procedia CIRP 87:159–163. https://doi.org/10.1016/j.procir.2020.02.031
23. Wang X, Zheng H, Wan Y et al (2018) Picosecond laser surface texturing of a stavax steel substrate for wettability control. Engineering 4:816–821. https://doi.org/10.1016/j.eng.2018.10.006

24. Wang XC, Wang B, Xie H et al (2018) Picosecond laser micro/nano surface texturing of nickel for superhydrophobicity. J Phys Appl Phys 51:115305. https://doi.org/10.1088/1361-6463/aaad24
25. Gan Z, Peng X, Guan C (2019) Machining of optical micro-mold by laser-induced chemical etching. AIP Adv 9:055106. https://doi.org/10.1063/1.5095590
26. Guo R, Qi L, Xu L et al (2021) Fabrication of 2D silicon nano-mold by side etch lift-off method. Nanotechnology 32:285301. https://doi.org/10.1088/1361-6528/abf50e
27. Iwai K, Shih KC, Lin X et al (2014) Finger-powered microfluidic systems using multilayer soft lithography and injection molding processes. Lab Chip 14:3790–3799. https://doi.org/10.1039/C4LC00500G
28. Ayoib A, Hashim U, Arshad MM, Thivina V (2016) Soft lithography of microfluidics channels using SU-8 mould on glass substrate for low cost fabrication. In: 2016 IEEE EMBS Conference on Biomedical Engineering and Sciences (IECBES). IEEE, pp 226–229. https://doi.org/10.1109/IECBES.2016.7843447
29. Hung J-C, Chang D-H, Chuang Y (2012) The fabrication of high-aspect-ratio micro-flow channels on metallic bipolar plates using die-sinking micro-electrical discharge machining. J Power Sources 198:158–163. https://doi.org/10.1016/j.jpowsour.2011.09.065
30. Chae J, Park SS, Freiheit T (2006) Investigation of micro-cutting operations. Int J Mach Tools Manuf 46:313–332. https://doi.org/10.1016/j.ijmachtools.2005.05.015
31. Behroodi E, Latifi H, Bagheri Z et al (2020) A combined 3D printing/CNC micro-milling method to fabricate a large-scale microfluidic device with the small size 3D architectures: an application for tumor spheroid production. Sci Rep 10:1–14. https://doi.org/10.1038/s41598-020-79015-5
32. Zhang Z, Peng H, Yan J (2013) Micro-cutting characteristics of EDM fabricated high-precision polycrystalline diamond tools. Int J Mach Tools Manuf 65:99–106. https://doi.org/10.1016/j.ijmachtools.2012.10.007
33. Ning F, Cong W (2020) Ultrasonic vibration-assisted (UV-A) manufacturing processes: state of the art and future perspectives. J Manuf Process 51:174–190. https://doi.org/10.1016/j.jmapro.2020.01.028
34. Wen J, Tang J, Zhou W (2021) Study on formation mechanism and regularity of residual stress in ultrasonic vibration grinding of high strength alloy steel. J Manuf Process 66:608–622. https://doi.org/10.1016/j.jmapro.2021.04.040
35. Xiao X, Zheng K, Liao W, Meng H (2016) Study on cutting force model in ultrasonic vibration assisted side grinding of zirconia ceramics. Int J Mach Tools Manuf 104:58–67. https://doi.org/10.1016/j.ijmachtools.2016.01.004
36. Gao T, Zhang X, Li C et al (2020) Surface morphology evaluation of multi-angle 2D ultrasonic vibration integrated with nanofluid minimum quantity lubrication grinding. J Manuf Process 51:44–61. https://doi.org/10.1016/j.jmapro.2020.01.024
37. Zhao Q, Sun Z, Guo B (2016) Material removal mechanism in ultrasonic vibration assisted polishing of micro cylindrical surface on SiC. Int J Mach Tools Manuf 103:28–39. https://doi.org/10.1016/j.ijmachtools.2016.01.003
38. Guo J, Feng W, Jong HJH et al (2020) Finishing of rectangular microfeatures by localized vibration-assisted magnetic abrasive polishing method. J Manuf Process 49:204–213. https://doi.org/10.1016/j.jmapro.2019.11.026
39. Cao Z-C, Cheung CF (2014) Theoretical modelling and analysis of the material removal characteristics in fluid jet polishing. Int J Mech Sci 89:158–166. https://doi.org/10.1016/j.ijmecsci.2014.09.008
40. Zhang Z, Cheung C, Wang C et al (2023) Modelling of surface morphology and roughness in fluid jet polishing. Int J Mech Sci 242:107976. https://doi.org/10.1016/j.ijmecsci.2022.107976
41. Zhang Z, Liu J, Hu W et al (2021) Chemical mechanical polishing for sapphire wafers using a developed slurry. J Manuf Process 62:762–771. https://doi.org/10.1016/j.jmapro.2021.01.004
42. Liu D, Zhang Z, Feng J et al (2023) Environment-friendly chemical mechanical polishing for copper with atomic surface confirmed by transmission electron microscopy. Colloids Surf A 656:130500. https://doi.org/10.1016/j.colsurfa.2022.130500
43. Zhang Z, Jin Z, Guo J et al (2019) A novel chemical mechanical polishing slurry for yttrium aluminum garnet crystal. Appl Surf Sci 496:143601. https://doi.org/10.1016/j.apsusc.2019.143601
44. Suzuki H, Okada M, Yamagata Y et al (2012) Precision grinding of structured ceramic molds by diamond wheel trued with alloy metal. CIRP Ann 61:283–286. https://doi.org/10.1016/j.cirp.2012.03.063
45. Guo J, Liu K, Wang Z, Tnay GL (2017) Magnetic field-assisted finishing of a mold insert with curved microstructures for injection molding of microfluidic chips. Tribol Int 114:306–314. https://doi.org/10.1016/j.triboint.2017.04.019
46. Kim W-B, Lee S-H, Min B-K (2005) Surface finishing and evaluation of three-dimensional silicon microchannel using magnetorheological fluid. J Manuf Sci Eng 126:772–778. https://doi.org/10.1115/1.1811113
47. Wang Y, Wu Y, Nomura M (2016) Feasibility study on surface finishing of miniature V-grooves with magnetic compound fluid slurry. Precis Eng 45:67–78. https://doi.org/10.1016/j.precisioneng.2016.01.010
48. Wang C, Zhang Z, Cheung CF et al (2022) Maskless fluid jet polishing of optical structured surfaces. Precis Eng 73:270–283. https://doi.org/10.1016/j.precisioneng.2021.09.010
49. Beaucamp A, Namba Y, Freeman R (2012) Dynamic multiphase modeling and optimization of fluid jet polishing process. CIRP Ann 61:315–318. https://doi.org/10.1016/j.cirp.2012.03.073
50. Zhang Z, Wang C, Cheung C et al (2023) Numerical and experimental investigation on the effect of surface curvature and slope angle on the material removal characteristics in fluid jet polishing. Int J Mech Sci 249:108266
51. Wang CJ, Cheung CF, Ho LT et al (2021) Development of a fluid line-jet polishing process for rotational axisymmetric surfaces. J Manuf Process 61:15–24. https://doi.org/10.1016/j.jmapro.2020.10.069
52. Haghbin N, Ahmadzadeh F, Papini M (2018) Masked micro-channel machining in aluminum alloy and borosilicate glass using abrasive water jet micro-machining. J Manuf Process 35:307–316. https://doi.org/10.1016/j.jmapro.2018.08.017
53. Wang CJ, Cheung CF, Ho LT et al (2017) A novel multi-jet polishing process and tool for high-efficiency polishing. Int J Mach Tools Manuf 115:60–73. https://doi.org/10.1016/j.ijmachtools.2016.12.006
54. Zhang Z, Cheung C, Wang C et al (2022) Restraint of the mid-spatial frequency error on optical surfaces by multi-jet polishing. Opt Express 26(30):46307–46323. https://doi.org/10.1364/OE.473235
55. Chen X, Brian Rowe W (1996) Analysis and simulation of the grinding process. Part II: Mechanics of grinding. Int J Mach Tools Manuf 36:883–896. https://doi.org/10.1016/0890-6955(96)00117-4
56. Wang CJ, Cheung CF, Ho LT, Loh YM (2020) An investigation of effect of stand-off distance on the material removal characteristics and surface generation in fluid jet polishing. Nanomanufacturing Metrol 3:112–122. https://doi.org/10.1007/s41871-020-00066-3